Ab initio calculation of the migration free energy of oxygen diffusion in pure and samarium-doped ceria

Julius Koettgen,[1,*] Peter C. Schmidt,[2] Tomáš Bučko,[3] and Manfred Martin[1,4,5,6,†]

[1]*Institute of Physical Chemistry, RWTH Aachen University, Landoltweg 2, 52056 Aachen, Germany*

[2]*Eduard-Zintl-Institut, Technische Universität Darmstadt, Alarich-Weiss-Strasse 8, Darmstadt, Germany*

[3]*Department of Physical and Theoretical Chemistry, Faculty of Natural Sciences, Comenius University in Bratislava, Mlynská Dolina,*
SK-84215 Bratislava, Slovakia and Institute of Inorganic Chemistry, Slovak Academy of Sciences, Dúbravská cesta 9,
SK-84236 Bratislava, Slovakia

[4]*JARA-HPC, Forschungszentrum Jülich and RWTH Aachen University, Germany*

[5]*JARA-Energy, Forschungszentrum Jülich and RWTH Aachen University, Germany*

[6]*Helmholtz-Institut Münster (IEK-12), Forschungszentrum Jülich GmbH, Corrensstr. 46, 48149 Münster, Germany*

We have studied the free energy migration barriers $\Delta F^{\ddagger}$ for oxygen diffusion in pure ceria and Sm-doped ceria for the temperatures 300, 700, and 1000 K. We used the density functional theory in the generalized gradient approximation and an additional Hubbard U parameter for the Ce $4f$ electronic states. We compare the results for the free energy deduced from three different methods. First, a static harmonic approach is applied in which the temperature dependent vibrational contributions to energy and entropy are deduced from the phonon frequencies of supercells with a fixed volume. Second, a static quasiharmonic approach is used in which a part of the anharmonicity effect is introduced via an implicit dependence of the harmonic frequencies on the thermally expanding cell volume. Third, the free energy barriers are calculated using metadynamics and molecular dynamics in which anharmonicity effects are naturally taken into account. The three methods examined in this study lead to distinctly different results. According to the harmonic approximation, the migration free energy difference $\Delta F^{\ddagger}$ increases with increasing temperature due to an increasing entropic contribution. According to the quasiharmonic approximation, the migration free energy is independent of temperature. Finally, molecular dynamics predicts a thermally induced increase in the migration free energy. We conclude that temperature dependent experimental lattice constants cancel out the increasing entropic contribution with increasing temperature in the static quasiharmonic approach. The full consideration of anharmonicity effects in the metadynamics method again leads to a temperature dependent migration free energy.

I. INTRODUCTION

The simulations of activated processes, which play an important role in chemistry and materials physics, have until recently been limited to the static approach based on atomic relaxations, sometimes followed by the analysis of the potential energy surface near the relevant stationary points via the harmonic approximation. However, the applicability of the harmonic approximation is restricted, especially at high temperatures [1–3]. More accurate schemes, in which the relevant thermodynamic quantities, most prominently the free energy, are computed by sampling the appropriate statistical ensembles, have been developed as early as in the 1970s [4]. Yet, until recently, they were used only within the framework of force field simulations. Although the computational power commonly available today allows us to combine these approaches with the quantum-mechanical calculation of forces [5], the applications to the "real-world" problems are still scarce and the old-fashioned static approach still dominates the realm of computational chemistry and materials physics.

In this paper, we apply three methods differing in the level of approximation to the transition state theory (TST) to study the temperature-dependent free energy of migration or migration free energy for defect diffusion in pure and doped ceria (CeO_2). The simplest of the methods that we examine is a static approach in which all degrees of freedom of the crystal are approximated by harmonic oscillators. We note that this approach was applied in our previous work [6]. In the next method, termed hereafter quasiharmonic approach, a part of the anharmonic effects is taken into account via an implicit dependence of the harmonic vibrational frequencies on the volume of the supercell, which is expanded with temperature [7–10]. Finally, we examine the molecular dynamics (MD) approach in which no presumption on the type of degrees of freedom is made and no *a priori* partitioning into vibrational, rotational, or translational degrees of freedom is needed [11]. One possible strategy to overcome the timescale problem occurring in molecular dynamics of activated processes, which are rare events, is the use of a bias potential accelerating the movement along the reaction path [12,13]. The bias potential can be chosen in different ways [14–16].

---

*julius.koettgen@rwth-aachen.de

†martin@rwth-aachen.de

In this paper, we use the metadynamics method [17,18] as implemented in the Vienna *ab initio* simulation package (VASP) [19].

Doped ceria exhibits a high oxygen ion conductivity and is a promising candidate for applications related to energy conversion and storage, where pure cerium oxide itself does not have a sufficient ionic conductivity [20]. Doping with lower valent oxides, like rare-earth oxides, creates oxygen vacancies resulting in a significant increase in oxygen ion conductivity. In particular, doping with samarium oxide (Sm_2O_3) leads to high conductivities as revealed by impedance spectroscopy experiments [21]. The ionic conductivity in doped ceria is investigated extensively by experimental methods [22]. Additionally, pure and doped ceria have been the subjects of numerous first-principles calculations [23–36] and kinetic Monte Carlo (KMC) simulations [34–44] including the calculation of the ionic conductivity and we review these results in our upcoming paper [45].

Theoretically, the electronic structure of ceria has been studied by density functional theory (DFT) using various exchange-correlation potentials. An overview of studies of this category is given by Loschen *et al.* [46]. It follows from results of these studies that a reasonable choice of the exchange-correlation potential seems to be the generalized gradient approximation (GGA) combined with an additional Hubbard U parameter [47], and the same approach is adopted also in this work.

Entropic terms have been found to be crucial for ceria: the catalytic application of ceria depends on its oxygen storage capacity and the reduction of Ce^{4+} cations to Ce^{3+} cations. Here, a large solid-state entropy of reduction can significantly increase the performance as shown by Meredig and Wolverton [48]. The entropy of reduction includes the electronic and ionic configurational entropy of ceria [49,50], the vibrational entropy of reduction [51], and the gas phase entropy. Naghavi *et al.* report a large positive onsite electronic configurational entropy, which arises from coupling between orbital and spin angular momenta in the lanthanide f orbital, explaining the excellent performance for high-temperature catalytic redox reactions [52]. For surface diffusion, Capdevila-Cortada and López report an entropic stabilization term for surfaces with a high number of empty sites using DFT calculations and molecular dynamics simulations [53].

The migration barrier of oxygen in ceria has been studied by both experimental and theoretical methods. The experimentally measured values of the activation barrier vary between about 0.5 eV and 0.9 eV [6,33,54]. The theoretically predicted migration barriers depend sensitively on computational details such as the exchange-correlation functional, lattice constant, the charged state of the migrating oxygen and the vacancy concentration [55]. The computed migration barriers vary roughly between 0.5 and 1 eV [6,31,35,56]. In cases where the migration barriers change with the local environment like in doped ceria, further steps are necessary to compare experimental and theoretical results as discussed in our earlier work [35].

This paper is organized as follows: the simulation methods used in this work are introduced in Sec. II, the simulation details are presented in Sec. III, the numerical results are presented in Sec. IV, and a summary of the results is given in Conclusion.

II. COMPUTATIONAL METHOD

A. Rate constant

Assume that the activated process of interest can be driven reversibly by changing the value of a continuous parameter ξ (reaction coordinate), that is, in general, a function of Cartesian coordinates $\boldsymbol{r}$ of all N atoms of the system. For simplicity, let us further assume that the reactant state (R) is defined by the condition $\xi \leqslant \xi_b$ and the inequality $\xi \geqslant \xi_b$ holds for the product state (P). The dividing surface ξ_b is the value of the reaction coordinate where the free energy barrier occurs. Following Eyring's transition state theory, the rate constant $\Gamma(T)$ for the transition $R \rightarrow P$ at the temperature T can be expressed by [57]

$$\Gamma(T) = \frac{\langle \dot{\xi} \theta(\dot{\xi}) \delta(\xi_b - \xi(0)) \rangle}{\langle \theta(\xi_b - \xi) \rangle}, \tag{1}$$

where $\dot{\xi}$ is the generalized velocity associated with the parameter ξ, θ is the Heaviside step function, δ is the delta function, $\xi(0)$ is the value of ξ at time $t = 0$, and angular brackets represent the NVT ensemble average. Next, we designate the free energy minimum on the reactant's side as ξ_a and rewrite Eq. (1) as follows:

$$\Gamma(T) = \frac{\langle |\dot{\xi}_b| \rangle}{2} P(\xi_a) e^{-\frac{\Delta F_{a \rightarrow b}}{k_B T}}, \tag{2}$$

whereby $\Delta F_{a \rightarrow b} = -k_B T \ln\{\frac{\langle \delta(\xi_b - \xi) \rangle}{\langle \delta(\xi_a - \xi) \rangle}\}$ is the reversible work needed to shift the value of ξ from ξ_a to ξ_b, and the term $P(\xi_a) = \frac{\langle \delta(\xi_a - \xi) \rangle}{\langle \theta(\xi_b - \xi) \rangle}$ is the probability density of the state $\xi(\boldsymbol{r}) = \xi_a$ within all reactant configurations. The former term can be computed, e.g., using metadynamics, as discussed below, while the latter contribution can be determined by straightforward molecular dynamics simulation. Although the term $\langle |\dot{\xi}_b| \rangle$ can be determined analytically for certain choices of ξ, such as Cartesian coordinates, in this work we rely on a more general numerical solution via the formula [58]

$$\langle |\dot{\xi}_b| \rangle = \frac{\langle Z^{-1/2} |\dot{\xi}| \rangle_{\xi_b}}{\langle Z^{-1/2} \rangle_{\xi_b}}, \tag{3}$$

where $\dot{\xi} = \sum_{i=1}^{N} \sum_{\mu=x,y,z} \frac{\partial \xi}{\partial r_{i,\mu}} \dot{r}_{i,\mu}$, the term enclosed in $\langle \ldots \rangle_{\xi_b}$ is computed as a constrained average with $\xi(\boldsymbol{r}) = \xi_b$ and the mass metric tensor is

$$Z = \sum_{i=1}^{N} \frac{1}{m_i} \sum_{\mu=x,y,z} \left(\frac{\partial \xi}{\partial r_{i,\mu}} \right)^2. \tag{4}$$

The rate constant can also be described by the Eyring-Polanyi equation [59,60]:

$$\Gamma(T) = \frac{k_B T}{h} e^{-\frac{\Delta F^{\ddagger}}{k_B T}}, \tag{5}$$

where $\Delta F^{\ddagger}$ is the migration free energy, which is in experiments referred to as free energy of activation [61]. By comparing Eq. (5) with Eq. (2), we find the relation between $\Delta F^{\ddagger}$ and $\Delta F_{a \rightarrow b}$:

$$\Delta F^{\ddagger} = \Delta F_{a \rightarrow b} - k_B T \cdot \ln \left(\frac{h}{k_B T} \frac{\langle |\dot{\xi}_b| \rangle}{2} P(\xi_a) \right). \tag{6}$$

The calculation of $\Delta F^{\ddagger}$ within the harmonic transition state theory approach (hTST) and quasiharmonic approach to TST (qhTST) are discussed in Sec. II D.

B. Metadynamics simulation

In metadynamics [17,18], a time-dependent bias potential $\tilde{V}(t,\xi)$ is added to the Lagrangian L driving molecular dynamics. The bias potential acts on a selected number of continuous geometric parameters. The collective variables $\xi(\boldsymbol{r})$ and the Lagrangian for metadynamics can be written as

$$\tilde{L}(\dot{\boldsymbol{r}},\boldsymbol{r},\xi,t) = L(\dot{\boldsymbol{r}},\boldsymbol{r}) - \tilde{V}[t,\xi(\boldsymbol{r}(t))]. \tag{7}$$

The bias potential is constructed by a sum of Gaussians of heights q and widths w,

$$\tilde{V}[t,\xi(\boldsymbol{r}(t))] = q \sum_{i=1}^{t/t_G} \exp\left[-\frac{|\xi(\boldsymbol{r}(t)) - \xi(\boldsymbol{r}(t_i))|^2}{2w^2} \right], \tag{8}$$

where t_G is a time increment for updating the bias potential. It can be shown that in the limit of infinitesimal height q and infinite time, the bias potential represents a negative image of the free-energy profile and the free-energy difference between the stable (a) and the transition state (b) can be obtained as

$$\Delta F_{a \to b} = -\lim_{t \to \infty} (\tilde{V}(t,\xi_b) - \tilde{V}(t,\xi_a)). \tag{9}$$

In practice, the negative of the bias potential accumulated during a metadynamics run represents an approximation of the true free energy profile. For more details about the method see, for example, the work by Bussi *et al.* [62]

C. Partitioning of the free energy using molecular dynamics

Having determined the value of the collective variable for the transition state (ξ_b) using metadynamics, the internal energy of activation $\Delta U^{\ddagger}$ can be computed as follows:

$$\Delta U^{\ddagger} = \frac{\langle Z^{-1/2} E \rangle_{\xi_b}}{\langle Z^{-1/2} \rangle_{\xi_b}} - \langle E \rangle_R, \tag{10}$$

where the first term on the right-hand side is the average energy of the transition state computed using constrained molecular dynamics with the value of ξ fixed at ξ_b. $\langle E \rangle_R$ is the average energy of the reactant state computed using standard molecular dynamics. The entropy of activation is then determined using the following thermodynamic relation:

$$\Delta S^{\ddagger} = \frac{\Delta U^{\ddagger} - \Delta F^{\ddagger}}{T}. \tag{11}$$

D. Harmonic and quasiharmonic approximation of the transition state theory

Within the static approach combined with the harmonic approximation, the Helmholtz migration free energy $\Delta F^{\ddagger}$ and its electronic and vibrational contributions $\Delta F_{el}^{\ddagger}$ and $\Delta F_{vib}^{\ddagger}$ are determined using the following formula:

$$\Delta F^{\ddagger} = \Delta F_{el}^{\ddagger} + \Delta F_{vib}^{\ddagger} = \underbrace{\Delta U_{el}^{\ddagger} + \Delta U_{vib}^{\ddagger}}_{\Delta U^{\ddagger}} - T \Delta S^{\ddagger}. \tag{12}$$

The electronic energy contribution for a singlet state for all systems discussed in this work is computed as the difference in potential energy between relaxed potential energy saddle point (b) and minimum (a):

$$\Delta F_{el}^{\ddagger} = \Delta U_{el}^{\ddagger} = E_{el,b} - E_{el,a}. \tag{13}$$

Similarly, the vibrational contributions to entropy and internal energy for a system with three-dimensional periodicity containing N atoms can be written as

$$\begin{aligned} \Delta U_{vib}^{\ddagger} &= U_{vib,b} - U_{vib,a}, \\ \Delta S_{vib}^{\ddagger} &= S_{vib,b} - S_{vib,a}, \end{aligned} \tag{14}$$

with

$$\begin{aligned} U_{vib,a}(T) &= \sum_{i=1}^{3N-3} \hbar\omega_i \left(\frac{1}{2} + \frac{1}{e^{\hbar\omega_i/k_B T} - 1} \right), \\ U_{vib,b}(T) &= \sum_{i=1}^{3N-4} \hbar\omega_i \left(\frac{1}{2} + \frac{1}{e^{\hbar\omega_i/k_B T} - 1} \right), \end{aligned} \tag{15}$$

and

$$\begin{aligned} S_{vib,a}(T) &= \sum_{i=1}^{3N-3} \left[\frac{\hbar\omega_i}{T} \frac{1}{e^{\hbar\omega_i/k_B T} - 1} - k_B \ln\left(1 - e^{-\frac{\hbar\omega_i}{k_B T}}\right) \right], \\ S_{vib,b}(T) &= \sum_{i=1}^{3N-4} \left[\frac{\hbar\omega_i}{T} \frac{1}{e^{\hbar\omega_i/k_B T} - 1} - k_B \ln\left(1 - e^{-\frac{\hbar\omega_i}{k_B T}}\right) \right]. \end{aligned} \tag{16}$$

In Eqs. (15) and (16), ω_i is the harmonic vibrational frequency of the ith vibrational mode, which is determined only at the Γ point in this work. It can be shown by taking the $h \to 0$ limit of Eq. (15) that the classical value of $\Delta U_{vib}^{\ddagger}$ is $-k_B T$. For the entropy, further contributions beyond S_{vib} are neglected in this work. We also note that whereas it holds that the higher the frequency the greater the contribution to the vibrational contribution to the internal energy, the opposite is true for the vibrational entropy, which tends to infinity for $\omega \to 0$ [see Eq. (16)].

Within the standard harmonic approximation, crystals do not expand when the temperature is raised. Thermal expansion of materials, on the other hand, leads to a significant variation of the harmonic vibrational frequencies used in Eqs. (15) and (16). The implicit dependency of harmonic frequencies on the volume (or some other appropriate parameter) is commonly used in the so-called quasiharmonic approaches to introduce an anharmonicity effect into simulations [63]. In the quasiharmonic approach (qhTST) used in this work, we use the experimentally measured expansion coefficient of CeO_2 to select appropriate cell volumes for different temperatures (see Sec. III A for details). For each such structure, the potential energies of the minimum and the saddle point, as well as the harmonic vibrational frequencies are determined, and we exploit these quantities to compute the free energies of activation via Eqs. (12)–(16).

III. COMPUTATIONAL DETAILS

A. Unit cell

Ceria CeO_2 crystallizes in the cubic $Fm\bar{3}m$ fluorite structure. In the harmonic approach, we use the lattice
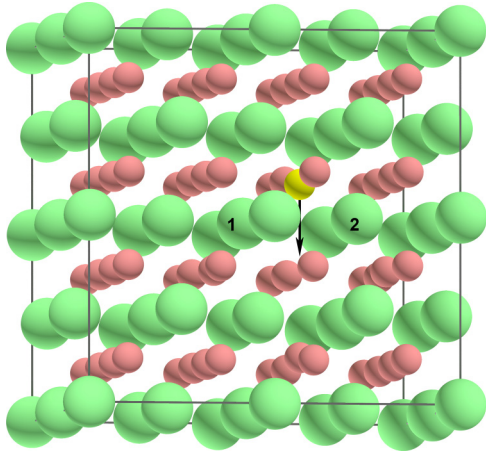
FIG. 1. $2 \times 2 \times 2$ supercell of pure ceria (large green: Ce; small red: O) with one oxygen vacancy used in our simulations. From the neutral crystal $Ce_{32}O_{64}$, we have taken out one O^{2-} at the position $(5/8;3/8;5/8)$ and created a charged unit cell $(Ce_{32}O_{63})^{2+}$ with an oxygen vacancy ($V_O^{\bullet\bullet}$). The diffusion path of $V_O^{\bullet\bullet}$ is along the y axis indicated by the black arrow. The diffusing oxygen O_m is marked yellow. The saddle point (transition state) is lying between the Ce atoms Ce_1 and Ce_2 ("migration edge"). For the doped system, the Ce atoms of the migration edge are replaced by Sm as sketched in Fig. 2.

constant obtained experimentally at room temperature, which is $a(300\,K) = 5.411\,Å$ [64], for all simulation temperatures. The lattice constant, however, increases significantly with increasing temperature; the linear thermal expansion coefficient of ceria is about $\alpha = 1.10 \cdot 10^{-5}\,K^{-1}$ [65–68]. For the temperatures of interest, one can deduce on the basis of the experimental data the following values of the lattice parameter: $a(700\,K) = 5.435\,Å$ and $a(1000\,K) = 5.453\,Å$. These lattice parameters are used in our quasiharmonic and molecular dynamics simulations. We have chosen a $2 \times 2 \times 2$ supercell of the cubic $Fm\bar{3}m$ fluorite structure with one oxygen vacancy, containing 95 atoms per unit cell, either $(Ce_{32}O_{63})^{2+}$ for pure ceria or $(Ce_{31}SmO_{63})^{1+}$ and $(Ce_{30}Sm_2O_{63})$ for the doped systems. Indeed, ceria can be easily reduced to $CeO_{2-\delta}$. Here, cerium ions Ce^{4+} are reduced to Ce^{3+} and oxygen vacancies are created. In our earlier publications, we already investigated the resulting formation of small polarons in reduced ceria [51,56,69]. However, in this work, we focus on ceria containing oxygen vacancies that are purely created by doping with lower valent oxides according to Eq. (17). We consider the pure ceria cell $(Ce_{32}O_{63})^{2+}$ as part of a larger cell of lightly doped ceria, where the two Sm^{3+} dopants are so far away from the vacancy that their effective interaction is negligible. Although charge-neutral cells containing defects without adjustment of the number of electrons would be preferable, the size of such cells would have to be very large leading to enormous computational times. Therefore charge-neutral cells with large distances between defects are virtually divided into oppositely charged cells. Charged cells are calculated by VASP assuming a neutralizing background charge, which is a valid approach, as shown in literature [70–73]. The supercell of pure ceria is shown in Fig. 1. The same supercells are used for the molecular dynamics and the static approach. We remark that doped ceria is investigated for the infinitely diluted cases and hence it is

justified to use the lattice constant of pure ceria also for such a system.

B. Electronic structure calculations

The density functional calculations were performed within the generalized gradient approximation (GGA) according to Perdew, Burke, and Ernzerhof [74] and the projector augmented wave (PAW) method, [75] as implemented in the Vienna *ab initio* simulation package (VASP) [76,77], which was used throughout this work. The electronic wave functions were expanded in a basis set of plane waves with a kinetic energy cutoff of $E_{kin} = 400\,eV$. A Hubbard U parameter was employed to account for localized Ce $4f$ electrons. A rotationally invariant approach [47] was used with an effective U parameter of $U = 5.0\,eV$ for the $4f$ orbitals of cerium, as recommended in literature [28,32–35,51,56,78–82].

Electronic calculations were carried out using a Γ-point sampling of the first Brillouin zone of the cubic supercell. Structural relaxations were conducted until the Hellmann-Feynman forces acting on all atoms were smaller than $0.005\,eV/Å$. The transition state was determined using the improved dimer method [83,84]. Phonon frequencies were calculated using the finite difference method [85].

The semi-core/valence electrons $5s^2 5p^6 6s^2 5d^1 4f^1$ of cerium, ($4f^5$ core) $5s^2 5p^6 6s^2 5d^1$ of samarium and $2s^2 2p^4$ of oxygen are taken as band electrons. The band-structure calculations show that the highest occupied valence states are the $2p$-like states of oxygen and the lowest conduction states are the $4f$-like states of cerium as discussed in earlier publications [25,33,78,86,87]. The position of the Fermi energy depends on the chosen charge state of the vacancy. We assume the following doping relationship:

$$Sm_2O_3 \xrightarrow{CeO_2} 2\,Sm_{Ce}' + V_O^{\bullet\bullet} + 3\,O_O^x, \qquad (17)$$
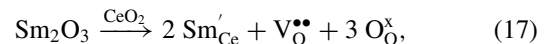
and the charged vacancies $V_O^{\bullet\bullet}$ are described by the unit cells $(Ce_{32}O_{63})^{2+}$, $(Ce_{31}SmO_{63})^{1+}$, and $(Ce_{30}Sm_2O_{63})^0$. For all three systems, the Fermi energy is lying in the band gap between the $2p$-like states of oxygen and the $4f$-like states of cerium.

C. Molecular dynamics

The computational setup related to the calculation of energies and forces is identical in molecular dynamics simulations and static calculations. Molecular dynamics simulations were performed using a 2 fs integration time step. The simulation temperature was controlled using a Nose-Hoover thermostat [88,89]. The internal energy of migration or migration internal energy was calculated using straightforward (initial state) or constrained (transition state) molecular dynamics by averaging the potential energy from at least 30 ps production runs, which followed equilibration runs of 10 ps. We note that the mass metric tensor [see Eq. (4)] associated with our choice of the collective variable is a constant and hence the position-dependent quantities can be computed from constrained averages directly without any unbiasing. For the metadynamics calculations, we use $t_G \approx 50$ time steps [see Eq. (8)]. In order to reduce the simulation time of the metadynamics calculations, we used an initial bias potential determined by fitting the potential energy
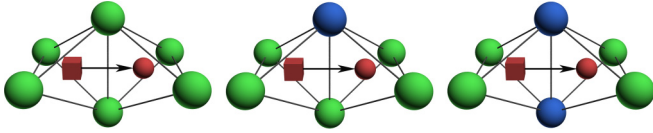
FIG. 2. Assumed migration edge configurations in samarium-doped ceria. Ce-Ce edge (left), Ce-Sm edge (middle), and Sm-Sm edge (right). Cerium ions (green), samarium ions (blue), oxygen ions (red spheres), and oxygen vacancies (red cubes).

profile from static calculations by five Gaussian functions. The metadynamics parameters q and w [see Eq. (8)] were initially set to the 0.01 eV and 0.02 Å. The value of q has been reduced to at least 0.001 eV during the simulation in order to improve the accuracy of the computed free energy profile. The calculations were terminated when the difference between the minimum and the maximum of $-\tilde{V}(\xi)$ was stable within 0.01 eV.

In Figs. 1 and 2, the diffusion path is indicated by arrows. This path is parallel to the Cartesian y axis and, therefore, it is natural to involve the y coordinates of atoms participating in diffusion in the definition of the collective variable ξ. In this work, the following form of ξ was used:

$$\xi(\boldsymbol{r}(t)) = y(O_m) - \frac{1}{2}[y(Ce_1) + y(Ce_2)], \qquad (18)$$

where $y(O_m)$ is the Cartesian coordinate y of the migrating oxygen, yellow in Fig. 1, and $y(Ce_1)$ and $y(Ce_2)$ are the Cartesian coordinates of the Ce ions at the migration edge, labeled 1 and 2 in Fig. 1. It follows from symmetry that the value of the collective variable in the transition state is $\xi_b = 0$ Å. The reference state ξ_a has been identified as the minimum on the free energy profile obtained from metadynamics. The corresponding probability density $P(\xi_a)$, which is needed to determine $\Delta F^\ddagger$ [Eq. (6)], as well as the total energy of the reactant $\langle E \rangle_R$, which is used in calculations of $\Delta U^\ddagger$ [Eq. (10)], have been obtained in a straightforward molecular dynamics run.

IV. RESULTS AND DISCUSSION

We have calculated the free energy barrier for the oxygen diffusion for the temperatures $T = 300$, 700, and 1000 K. All simulations have been performed for the systems $(Ce_{32}O_{63})^{2+}$, $(Ce_{31}SmO_{63})^{1+}$, and $(Ce_{30}Sm_2O_{63})^{0}$. In Sec. IV A, we give the results of the harmonic approach. These values will be compared to the quasiharmonic approach in Sec. IV B. Finally, the molecular dynamics studies are presented in Sec. IV C.

A. Harmonic approach

For a harmonic static approximation, which is the crudest approximation to the transition state theory considered in this work, the cell volume is kept constant at all temperatures (see Sec. III A). The atomic relaxation of the ions for $(Ce_{32}O_{63})^{2+}$ shows that in the equilibrium state the migrating oxygen ion O_m is shifted from the equilibrium position in the ideal CeO_2 lattice by about 0.2 Å towards the oxygen vacancy. In the transition state, the distance between O_m and the migration edge Ce ions is about 0.2 Å shorter than the Ce-O bonding distance in bulk

ceria in accordance with an earlier work. [6] The collective variable ξ has a value of $\xi_b \approx 0$ Å for the transition state and $\xi_a \approx -1.1$ Å for the initial state (Table III for 300 K). The difference in the collective variable between initial and transition state increases when the cerium ions are replaced by samarium ions at the migration edge.

For the Ce-Sm edge, the migrating oxygen ion moves away from the large Sm dopant in the transition state leading to a curved migration path. As a result, the surrounding ions give way for the displaced ions; in the same transition state, the oxygen ions and cations next to the migrating oxygen ion move away from the Sm dopant and move even further away from the migrating oxygen ion. For the Sm-Sm edge, again oxygen ions and cations next to the migrating oxygen ion and the migration edge make room for both the migrating oxygen ion and the migration edge cations. The relaxation around the migrating oxygen ion is significantly stronger for the Sm-Sm edge, where the largest electronic migration energy $\Delta U^\ddagger_{el,hTST}$ and migration entropy $\Delta S^\ddagger_{hTST}$ can be found.

The migration free energies and different contributions to this quantity determined using the harmonic transition state theory are compiled in Table I. We note that our result for $\Delta U^\ddagger_{el,hTST}$ in pure ceria is 0.15 eV larger than the value found earlier [78] for the same exchange-correlation potential. This difference occurs, as the used electron configurations are different. Nolan *et al.* [78] used $(Ce_{32}O_{63})^{0}$ instead of $(Ce_{32}O_{63})^{2+}$ and two Ce neighbored to the oxygen vacancy are reduced to Ce'_{Ce}. The values of $\Delta U^\ddagger_{el,hTST}$ reported here also moderately differ from our results published previously, which is caused by a different computational setup [6].

For instance, we found that the increase of the plane-wave cutoff from 400 to 500 eV or the increase of the number of k-points mentioned in Sec. III C changes the values for $\Delta U^\ddagger_{el,hTST}$ by less than 0.002 eV, whereas the increase of the unit cell from $2 \times 2 \times 2$ to $3 \times 3 \times 3$ decreases $\Delta U^\ddagger_{el,qhTST}$ by 0.04 eV. However, the introduction of the Hubbard U parameter ($U = 5.0$ eV), which accounts for the localized Ce 4f electrons, strongly increases $\Delta U^\ddagger_{el,hTST}$ by 0.13 eV at the same lattice parameter. In fact, a linear increase of $\Delta U^\ddagger_{el,hTST}$ as a function of the Hubbard U parameter can be found between a Hubbard U parameter of 0 eV and 10 eV in steps of 1 eV. Here, $\Delta U^\ddagger_{el,hTST}$ increases by 0.02 eV per 1 eV increase in the Hubbard U parameter. For the vibrational contributions to the free energy, no change in $\Delta U^\ddagger_{vib,hTST}$ can be found. The migration entropy $\Delta S^\ddagger_{hTST}$ decreases linearly with an increasing Hubbard U parameter between 0 eV and 5 eV by a factor of 0.5. For higher Hubbard U parameters up to 10 eV, $\Delta S^\ddagger_{hTST}$ is constant. The strong dependence of the free energy on the Hubbard U parameter emphasizes the importance of the choice of the Hubbard U parameter if an exact absolute value for the free energy is desired [32,35,46,51,56,82,90–95]. In qualitative agreement with our previous results [6], the temperature-independent electronic migration energy $\Delta U^\ddagger_{el,hTST}$ increases significantly along the Ce-Ce, Ce-Sm, and Sm-Sm series. A detailed discussion is also provided in other literature [26,31,35].

The vibrational contribution to the migration internal energy ($\Delta U^\ddagger_{vib,hTST}$) roughly follows the expected trend: The

TABLE I. Contributions to the migration free energy as functions of temperature in ceria and Sm-doped ceria obtained using the harmonic approximation of the TST. The experimental lattice constants of pure ceria at 300 K are used, see Section 3.1. All electronic contributions are calculated at zero temperature.

Migration edge	T (K)	$\Delta U^{\ddagger}_{\text{el,hTST}}$ (eV)	$\Delta U^{\ddagger}_{\text{vib,hTST}}$ (eV)	$\Delta U^{\ddagger}_{\text{hTST}}$ (eV)	$\Delta S^{\ddagger}_{\text{hTST}}$ (meV/K)	$\Delta F^{\ddagger}_{\text{vib,hTST}}$ (eV)	$\Delta F^{\ddagger}_{\text{hTST}}$ (eV)
Ce-Ce	300	0.70	−0.01	0.69	−0.08	0.01	0.71
	700	0.70	−0.05	0.65	−0.17	0.07	0.77
	1000	0.70	−0.08	0.62	−0.21	0.12	0.83
Ce-Sm	300	0.85	−0.02	0.84	−0.07	0.01	0.86
	700	0.85	−0.06	0.80	−0.16	0.05	0.91
	1000	0.85	−0.08	0.77	−0.19	0.11	0.96
Sm-Sm	300	1.19	−0.03	1.17	0.07	−0.05	1.14
	700	1.19	−0.06	1.13	0.00	−0.06	1.13
	1000	1.19	−0.09	1.11	−0.03	−0.06	1.14

absolute values increase with increasing temperature and the deviations from the classical value $-k_B T$ (see Sec. II D) decrease along the same direction. Hence, within the accuracy of our calculations, the term $\Delta U^{\ddagger}_{\text{vib,hTST}}$ is independent of the presence of Sm atoms at the migration edge. The computed zero-point energy (ZPE) is only 0.02 eV or less and hence this contribution can be neglected in practice [6,96]. We shall make use of this result in Sec. IV C where the molecular dynamics simulations with neglected ionic quantum effects are discussed.

The entropy term $-T \Delta S^{\ddagger}_{\text{hTST}}$ takes typically a positive value that is larger than the $\Delta U^{\ddagger}_{\text{vib,hTST}}$ term and hence it contributes to the increase of the migration free energy ($\Delta F^{\ddagger}_{\text{hTST}}$) with increasing temperature predicted by our simulations. The Sm-Sm system is anomalous in this sense: compared to the Ce-Ce and Ce-Sm systems, the presence of heavier Sm atoms leads to a softening of low-frequency vibrations in the transition state. This effect is evident from the inspection of the computed vibrational density of states (VDOS, see Fig. 3): while the VDOS computed for the initial state changes only slightly when the Ce atoms at the migration edge are replaced by two Sm atoms, the same substitution gives rise to a new peak centered at 1 THz, which is not present in the initial state

(see right panel of Fig. 3). As the low-frequency modes are the most significant contributors to the entropy (see Sec. II D) [97], we observe an increased entropy of the transition state and in turn also an increased $\Delta S^{\ddagger}_{\text{hTST}}$ as compared to Ce-Ce and Ce-Sm systems.

B. Quasiharmonic approach

The harmonic approximation discussed in Sec. IV A neglects the thermal expansion of materials. However, thermal expansion might be important especially if the target temperature is very different from the temperature at which the cell geometry has been determined. In the here-discussed quasiharmonic approach, this problem is addressed. The quasiharmonic approach includes a part of the anharmonicity effect via an implicit dependence of vibrational frequencies on the cell volume [63]. We note that the cell volumes used for all systems at $T = 300$ K are the same as those considered in the harmonic approach, hence all low temperature results presented in this section (Table II) are identical to those discussed in Sec. IV A. The thermal expansion affects the distances between the migration edge atoms only moderately: these parameters increase by 0.04 Å in the initial state and
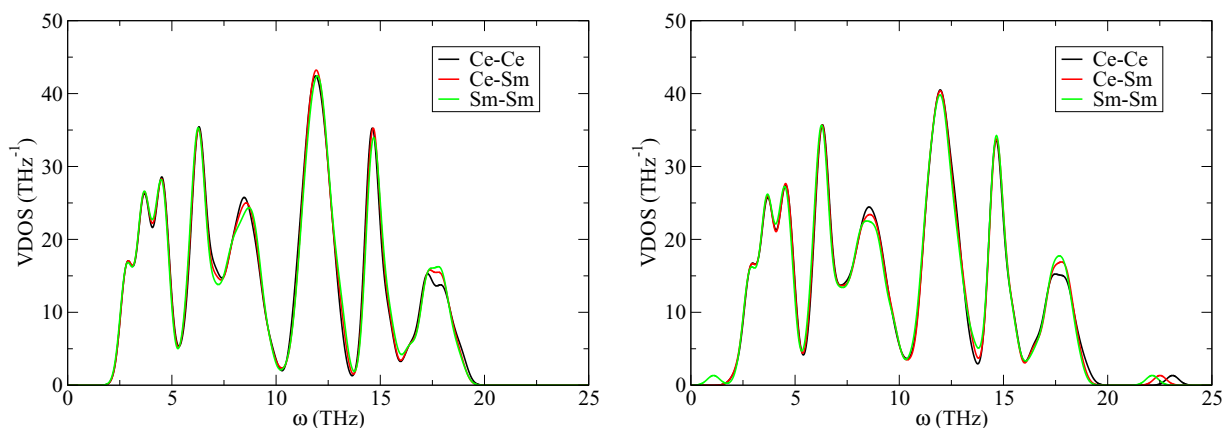

FIG. 3. Harmonic vibrational density of states as a function of the frequency computed for the initial state (left) and the transition state (right) of oxygen migration in the systems Ce-Ce, Ce-Sm, and Sm-Sm at 300 K.

TABLE II. Contributions to the migration free energy as functions of temperature in ceria and Sm-doped ceria obtained using the quasiharmonic approximation of the TST. The experimental lattice constants of pure ceria are used, see Sec. III A. All electronic contributions are calculated at zero temperature.

Migration edge	T (K)	$\Delta U_{\mathrm{el,qhTST}}^{\ddagger}$ (eV)	$\Delta U_{\mathrm{vib,qhTST}}^{\ddagger}$ (eV)	$\Delta U_{\mathrm{qhTST}}^{\ddagger}$ (eV)	$\Delta S_{\mathrm{qhTST}}^{\ddagger}$ (meV/K)	$\Delta F_{\mathrm{vib,qhTST}}^{\ddagger}$ (eV)	$\Delta F_{\mathrm{qhTST}}^{\ddagger}$ (eV)
Ce-Ce	300	0.70	−0.01	0.69	−0.10	0.02	0.72
	700	0.65	−0.06	0.59	−0.15	0.05	0.70
	1000	0.62	−0.08	0.53	−0.18	0.10	0.72
Ce-Sm	300	0.85	−0.02	0.84	−0.07	0.01	0.86
	700	0.81	−0.06	0.75	−0.16	0.06	0.86
	1000	0.77	−0.08	0.69	−0.21	0.13	0.90
Sm-Sm	300	1.19	−0.03	1.17	0.07	−0.05	1.14
	700	1.16	−0.06	1.10	−0.06	−0.02	1.14
	1000	1.13	−0.09	1.04	0.14[a]	−0.23[a]	0.90[a]

[a]For the Sm-Sm edge at 1000 K, the transition state is significantly more sensitive to noise in the vibrational spectra, which results in strong deviations in the vibrational data for this system.

0.03 Å in the transition state when the temperature is raised from 300 to 1000 K (see Table S1 in Ref. [98]). The value of the collective variable for the stable state, on the other hand, is almost unaffected, as shown in Table III. We note that the value of $\xi = 0$ Å in the transition state is fixed by the symmetry. A significant effect of the expansion is found for the term $\Delta U_{\mathrm{el,qhTST}}^{\ddagger}$, which decreases with increasing temperature (see Table II) and this correlation is approximately linear for all systems. The variation of $\Delta U_{\mathrm{el,qhTST}}^{\ddagger}$ with temperature is similar in magnitude to that of the temperature dependent terms analyzed in Sec. IV A. Hence we conclude that the electronic contribution to the temperature dependence of the migration free energy, which is completely neglected in the harmonic approach, is significant in the quasiharmonic approach.

As shown in Fig. 4, the vibrational frequencies decrease with increased temperature (redshift), which is a direct consequence of the lattice expansion [99]. Taking this variation in the vibrational spectra into account, it is remarkable that the computed values of the term $\Delta U_{\mathrm{vib,qhTST}}^{\ddagger}$ (Table III) are identical to those obtained using the harmonic approach. This result can be understood as follows: As mentioned in Sec. IV A, all systems are close to the classical behavior at high tem-

TABLE III. Positions of the free-energy minimum (ξ_{a}) determined in the static quasiharmonic approach.

Migration edge	T (K)	ξ_{a}/a	ξ_{a} (Å)
Ce-Ce	300	−0.197	−1.07
	700	−0.197	−1.06
	1000	−0.196	−1.06
Ce-Sm	300	−0.204	−1.10
	700	−0.204	−1.10
	1000	−0.204	−1.10
Sm-Sm	300	−0.214	−1.16
	700	−0.214	−1.16
	1000	−0.215	−1.16

perature and hence the term $\Delta U_{\mathrm{vib}}^{\ddagger}$ simply approaches $-k_{\mathrm{B}}T$, regardless of the cell volume. Of course, the explanation of the agreement between the harmonic approach and quasiharmonic approach for the lowest temperature considered here, where the most significant deviation from the classical behavior is to be expected, is trivial. In this case, identical cell geometries are used in both approaches and hence the results are the same. As before, the zero-point energy contributes only 0.02 eV or less to the migration free energy. An exception is the Sm-Sm 1000 K system for which the transition state is significantly more sensitive to noise in the vibrational spectra. Compared to the Ce-Ce or Ce-Sm edge at 1000 K, changes in the free energy of the Sm-Sm 1000 K transition state are about 6–60 times larger if individual vibrational frequencies are changed by 0.05 THz. Compared to the Ce-Ce or Ce-Sm edge at lower temperatures, this change can be one order of magnitude larger. Therefore, even a minor noise in the vibrational spectra results in strong deviations in the vibrational data for the Sm-Sm 1000-K system. For phonon calculations with an increased plane-wave cutoff of 500 eV, the migration free energies of the Sm-Sm 300-K and 1000-K systems are similar.

The vibrational entropy decreases with temperature, which is qualitatively the same result as obtained using the harmonic approach. This quantity sensitively reflects changes in the vibrational spectrum, especially in the low-frequency region. The comparison of the quasiharmonic and harmonic results does not suggest any obvious trend. As before, the Sm-Sm system behaves anomalously at 1000 K, whereby the term $\Delta S_{\mathrm{qhTST}}^{\ddagger}$ takes a large positive value and this problem is again attributed to the presence of a very low frequency peak in the VDOS for the Sm-Sm system, which is even redshifted at high temperature (see Fig. 4).

Interestingly, the temperature dependent terms tend to cancel each other largely and hence the migration free energy computed using the quasiharmonic approach changes only moderately with temperature and without any obvious trend. In fact, the computed $\Delta F_{\mathrm{qhTST}}^{\ddagger}$ is in most cases not very different from $\Delta U_{\mathrm{el,qhTST}}^{\ddagger}$ determined for 300 K. Hence the quasiharmonic approximation is in contrast to the harmonic approximation, which predicts a significant increase of $\Delta F_{\mathrm{TST}}^{\ddagger}$
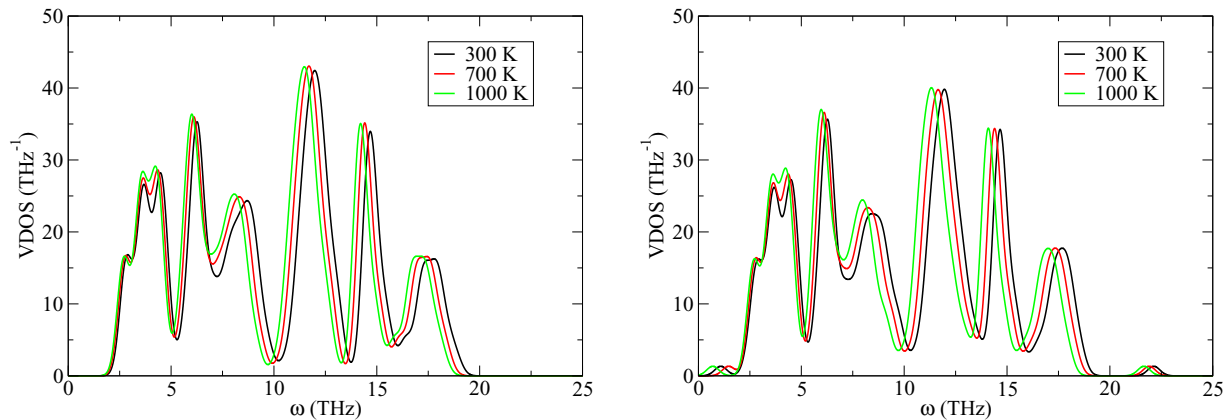
FIG. 4. Temperature-induced shift of the vibrational density of states computed using the quasiharmonic approximation for the Sm-Sm system: initial state (left), transition state (right).

with increasing temperature. In both cases, the Sm-Sm system is exception from trend as it behaves anomalously at increased temperature.

C. Molecular dynamics

The molecular dynamics based approach described in Sec. II B represents the most sophisticated method to compute free-energetics of activated processes examined in this study. As in the quasiharmonic approach, the thermal expansion of the lattice is taken into account but, in contrast to the quasiharmonic approach, the harmonic approximation is lifted and all atomic degrees of freedom are explicitly sampled. We note that the quantum effects, particularly the zero-temperature vibrations, are not taken into account in molecular dynamics but as we have shown in Secs. IV A and IV B, these effects contribute only negligibly to migration free energy at temperatures considered in this study.

The free-energy profiles $F(\xi)$ determined by metadynamics for the Ce-Ce edge, the Ce-Sm edge, and the Sm-Sm edge are shown in Fig. 5 as well as Figs. S1 and S2 in Ref. [98]. The position of the free energy minimum changes with temperature only moderately (Table IV), mostly as a consequence of the lattice expansion. According to our calculations, the term $\Delta F_{a\to b,\mathrm{MD}}$ [cf. Eq. (6)] is almost independent of temperature for all three edges under consideration and varies with temperature only within 0.02 eV (see Table V). A strong temperature dependence is introduced into the free energy barrier via the term $P(\xi_a)$, which decreases with increasing temperature (see Table IV, Fig. 6, and Figs. S3 and S4 in Ref. [98]). Although this contribution is partly compensated by the velocity term $\langle|\dot{\xi}_b|\rangle$ monotonically increasing with temperature (see Table IV), the overall effect is that the barrier $\Delta F_{\mathrm{MD}}^{\ddagger}$ increases for all systems by 0.13 eV to 0.16 eV as the temperature is raised
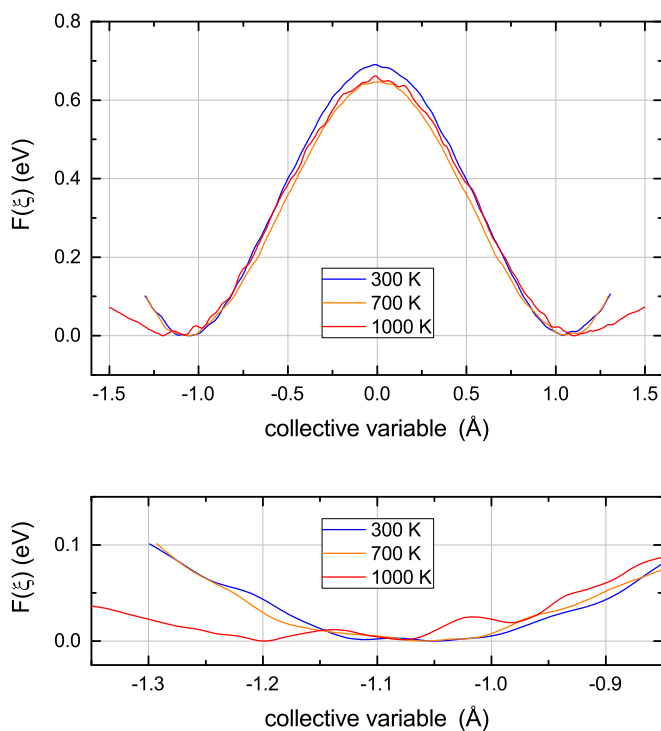

FIG. 5. Free energy profiles for the jump of a migrating oxygen ion for the Ce-Ce edge for different temperatures, $T = 300, 700$, and 1000 K. In the bottom figure, an excerpt of the upper data is shown.

TABLE IV. Computed values of quantities employed in the free-energy calculations using molecular dynamics (see Sec. II in the main text). We note that the free-energy profiles obtained in metadynamics were symmetrized.

Migration edge	T (K)	ξ_a (Å)	$P(\xi_a)$ (Å^{-1})	$|\dot{\xi}_b|$ (Å/fs)
Ce-Ce	300	−1.04	4.2	1.19
	700	−1.05	2.8	1.82
	1000	−1.09	2.4	2.18
Ce-Sm	300	−1.10	4.6	1.18
	700	−1.10	3.1	1.80
	1000	−1.11	2.6	2.15
Sm-Sm	300	−1.13	4.6	1.50
	700	−1.13	3.2	1.75
	1000	−1.14	2.6	2.11

TABLE V. Contributions to the migration free energy deduced from molecular dynamics as functions of temperature in ceria and Sm-doped ceria. The temperature dependent experimental lattice constants are used for the simulation, see Sec. III A.

Migration edge	T (K)	$\Delta U_{MD}^{\ddagger}$ (eV)	$\Delta S_{MD}^{\ddagger}$ (meV/K)	$\Delta F_{a \to b, MD}$ (eV)	$\Delta F_{MD}^{\ddagger}$ (eV)
Ce-Ce	300	0.69	−0.06	0.68	0.71
	700	0.63	−0.17	0.65	0.75
	1000	0.58	−0.26	0.66	0.84
Ce-Sm	300	0.84	−0.14	0.86	0.88
	700	0.78	−0.24	0.85	0.95
	1000	0.74	−0.27	0.84	1.01
Sm-Sm	300	1.17	0.18	1.10	1.12
	700	1.14	−0.07	1.09	1.19
	1000	1.09	−0.18	1.10	1.28

from 300 to 1000 K. This result is in a striking contrast to our quasiharmonic approach analysis. Curiously, however, the molecular dynamics results for the Ce-Ce and Ce-Sm systems are surprisingly similar to those of our harmonic approach calculations, where all anharmonic effects are completely neglected. As expected from the results presented in Sec. IV A and IV B, the migration free energy increases by about 0.2 eV per substitution of a cerium ion at the migration edge by a samarium ion.

The migration internal energy $\Delta U_{MD}^{\ddagger}$ determined by molecular dynamics is presented in Table V. For increasing temperature, the migration internal energy follows the opposite trend than $\Delta F^{\ddagger}$: the computed values decrease by 0.08 to 0.11 eV when the temperature is increased from 300 to 1000 K. We note that the numerical values of $\Delta U_{MD}^{\ddagger}$ correlate with the electronic contribution to the migration energy identified using the harmonic and quasiharmonic approaches. When cerium ions are replaced by samarium ions at the migration edge, the term $\Delta U_{MD}^{\ddagger}$ increases by a similar amount as $\Delta F_{MD}^{\ddagger}$.

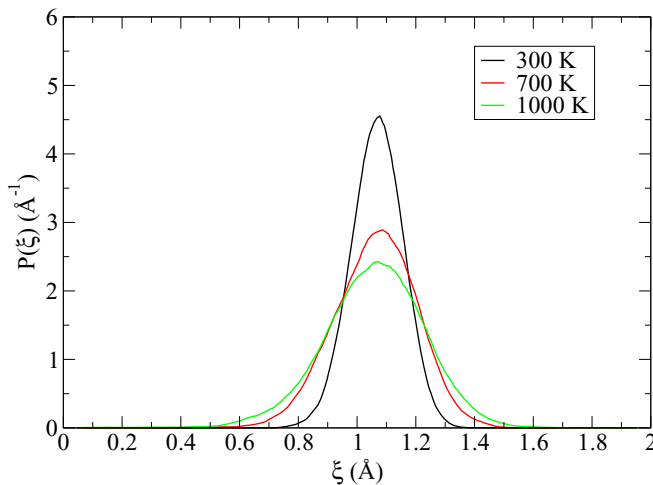

FIG. 6. Probability density for the reaction coordinate (ξ) computed for the reactant configuration of the Ce-Ce edge.

The migration entropies $\Delta S_{MD}^{\ddagger}$ were computed as described in Sec II C. Because the migration free energy $\Delta F^{\ddagger}$ and the migration internal energy $\Delta U^{\ddagger}$ exhibit opposite thermal trends, $\Delta S_{MD}^{\ddagger}$ decreases to larger negative values with increasing temperature as shown in Table V. This trend is in qualitative agreement with the harmonic and quasiharmonic approach results, although the numerical values are significantly different in most cases.

V. CONCLUSION

We investigated the free-energy migration barriers for the oxygen diffusion in ceria and Sm-doped ceria by three different methods: in the harmonic approach, static calculations for the total energy and phonon analyses in harmonic approximation are combined. The experimental lattice constant of pure ceria at 300 K was used for all calculations. In the quasiharmonic approach, thermal expansion was additionally taken into account for both the static calculations and the phonon analyses. In the metadynamics simulation, a bias potential built on-the-fly is used to determine the free-energy migration barrier. Again, thermally expanding experimental lattice constants were considered.

Anharmonicity effects are treated differently by each method. Going from the harmonic to the quasiharmonic approach, the anharmonicity effects associated with the thermal expansion of the material are added. When shifting further to molecular dynamics, the harmonic approximation is lifted completely. However, zero-temperature vibrations are not taken into account in the latter method, which contribute by 0.02 eV or less to the migration free energy according to the quasiharmonic approach.

The migration free energies derived from all methods differ significantly, especially at the highest temperature. According to the harmonic approximation, i.e., with a temperature independent lattice parameter and therefore a temperature independent electronic migration energy, the migration free energy difference $\Delta F^{\ddagger}$ increases with increasing temperature due to the entropic contribution. According to the quasiharmonic approximation, the migration free energy is independent of temperature. The main reason for the temperature independence of the free energy is the cancelation between the electronic migration energy contribution decreasing and the $-T \Delta S_{qhTST}^{\ddagger}$ term increasing with temperature. Finally, the migration free energy computed using molecular dynamics increases with increasing temperature.

A comparison to experimental data could help to verify the best theoretical method. However, the scattering of experimental values of the apparent migration entropy extracted from conductivity measurements is larger than the differences in migration entropy between the theoretical methods [6,100]. Furthermore, nominal pure ceria in experiments still contains very small amounts of impurities. As shown in our earlier publication, even very small concentrations of dopants that lead to strong dopant-oxygen vacancy-associates significantly increase the apparent migration entropy, which is extracted from conductivity measurements at temperatures below 1000 K [6]. Both reasons impede a comparison of the migration entropy with experiments.

From a practical point of view, static calculations and phonon analyses are significantly less computationally demanding than molecular dynamics simulations. However, static calculations fail for complex transition-state geometries as shown in this work for the Sm-Sm edge at 1000 K. Here, molecular dynamics is a more robust alternative.

The main aim of this work is to demonstrate that the metadynamics procedure is a powerful tool to study diffusion processes in oxides. Within this method, the restrictions of the harmonic approximation, such as the presumed shape of the potential energy surface and the decoupling of vibrational modes, are lifted and by choosing appropriate collective variables, even complex diffusion jumps can be taken into account. The metadynamics procedure might even be useful for amorphous systems if it is possible to define the initial and final states clearly in terms of one or a few structure descriptors or internal coordinates.

[1] A. Glensk, B. Grabowski, T. Hickel, and J. Neugebauer, Phys. Rev. X **4**, 011018 (2014).

[2] A. Glensk, B. Grabowski, T. Hickel, and J. Neugebauer, Phys. Rev. Lett. **114**, 195901 (2015).

[3] B. Vlaisavljevich *et al.*, J. Phys. Chem. A **121**, 4139 (2017).

[4] C. Chipot and A. Pohorille, *Free Energy Calculations*, Theory and Applications in Chemistry and Biology Vol. 86 (Springer-Verlag, Berlin, Heidelberg, 2007).

[5] J. Neugebauer and M. Asta, Phys. Status Solidi B **245**, 2617 (2008).

[6] J. Koettgen, T. Zacherle, S. Grieshammer, and M. Martin, Phys. Chem. Chem. Phys. **19**, 9957 (2017).

[7] A. van de Walle and G. Ceder, Rev. Mod. Phys. **74**, 11 (2002).

[8] G. Grimvall, B. Magyari-Köpe, V. Ozoliņš, and K. A. Persson, Rev. Mod. Phys. **84**, 945 (2012).

[9] M. Asta and V. Ozoliņš, Phys. Rev. B **64**, 094104 (2001).

[10] M. Youssef, B. Yildiz, and K. J. van Vliet, Phys. Rev. B **95**, 161110(R) (2017).

[11] R. Car, P. Blöchl, and E. Smargiassi, MSF **83–87**, 433 (1992).

[12] R. LeSar and D. C. Chrzan, Mater. Today **2**, 21 (1999).

[13] Y. Shin and K. A. Persson, ACS Appl. Mater. Interfaces **8**, 25595 (2016).

[14] A. F. Voter, J. Chem. Phys. **106**, 4665 (1997).

[15] M. M. Steiner, P.-A. Genilloud, and J. W. Wilkins, Phys. Rev. B **57**, 10236 (1998).

[16] R. A. Miron and K. A. Fichthorn, J. Chem. Phys. **119**, 6210 (2003).

[17] A. Laio and M. Parrinello, Proc. Natl. Acad. Sci. U. S. A. **99**, 12562 (2002).

[18] M. Iannuzzi, A. Laio, and M. Parrinello, Phys. Rev. Lett. **90**, 238302 (2003).

[19] T. Bucko, J. Phys.: Condens. Matter **20**, 064211 (2008).

[20] M. Panhans and R. Blumenthal, Solid State Ionics **60**, 279 (1993).

[21] K. Eguchi, T. Setoguchi, T. Inoue, and H. Arai, Solid State Ionics **52**, 165 (1992).

[22] M. Mogensen, Solid State Ionics **129**, 63 (2000).

[23] H. Yoshida, Solid State Ionics **160**, 109 (2003).

[24] N. V. Skorodumova, M. Baudin, and K. Hermansson, Phys. Rev. B **69**, 075401 (2004).

[25] Z. Yang, T. K. Woo, M. Baudin, and K. Hermansson, J. Chem. Phys. **120**, 7741 (2004).

[26] D. A. Andersson, S. I. Simak, N. V. Skorodumova, I. A. Abrikosov, and B. Johansson, Proc. Natl. Acad. Sci. U. S. A. **103**, 3518 (2006).

[27] C. Frayret, A. Villesuzanne, M. Pouchard, F. Mauvy, J.-M. Bassat, and J.-C. Grenier, J. Phys. Chem. C **114**, 19062 (2010).

[28] A. Ismail, J. Hooper, J. B. Giorgi, and T. K. Woo, Phys. Chem. Chem. Phys. **13**, 6116 (2011).

[29] A. Chroneos, B. Yildiz, A. Tarancón, D. Parfitt, and J. A. Kilner, Energy Environ. Sci. **4**, 2774 (2011).

[30] K. Muthukkumaran, R. Bokalawela, T. Mathews, and S. Selladurai, J. Mater. Sci. **42**, 7461 (2007).

[31] M. Nakayama and M. Martin, Phys. Chem. Chem. Phys. **11**, 3241 (2009).

[32] P. P. Dholabhai, J. B. Adams, P. Crozier, and R. Sharma, Phys. Chem. Chem. Phys. **12**, 7904 (2010).

[33] P. P. Dholabhai, J. B. Adams, P. Crozier, and R. Sharma, J. Chem. Phys. **132**, 094104 (2010).

[34] P. P. Dholabhai and J. B. Adams, J. Mater. Sci. **47**, 7530 (2012).

[35] S. Grieshammer, B. O. H. Grope, J. Koettgen, and M. Martin, Phys. Chem. Chem. Phys. **16**, 9974 (2014).

[36] J. O. Nilsson, M. Leetmaa, O. Y. Vekilova, S. I. Simak, and N. V. Skorodumova, Phys. Chem. Chem. Phys. **19**, 13723 (2017).

[37] A. Murray, G. Murch, and C. Catlow, Solid State Ionics **18–19**, 196 (1986).

[38] S. B. Adler and J. W. Smith, Faraday Trans. **89**, 3123 (1993).

[39] M. Meyer and N. Nicoloso, Berichte der Bunsen-Gesellschaft **101**, 1393 (1997).

[40] P. P. Dholabhai, S. Anwar, J. B. Adams, P. Crozier, and R. Sharma, J. Solid State Chem. **184**, 811 (2011).

[41] P. P. Dholabhai, J. B. Adams, P. A. Crozier, and R. Sharma, J. Mater. Chem. **21**, 18991 (2011).

[42] A. Oaks, Di Yun, B. Ye, W.-Y. Chen, and J. F. Stubbins, J. Nucl. Mater. **414**, 145 (2011).

[43] P. P. Dholabhai, S. Anwar, J. B. Adams, P. A. Crozier, and R. Sharma, Modelling Simul. Mater. Sci. Eng. **20**, 015004 (2012).

[44] B. O. H. Grope, T. Zacherle, M. Nakayama, and M. Martin, Solid State Ionics **225**, 476 (2012).

[45] J. Koettgen, S. Grieshammer, P. Hein, B. O. H. Grope, M. Nakayama, and M. Martin (unpublished).

[46] C. Loschen, J. Carrasco, K. Neyman, and F. Illas, Phys. Rev. B **75**, 035115 (2007).

[47] S. L. Dudarev, G. A. Botton, S. Y. Savrasov, C. J. Humphreys, and A. P. Sutton, Phys. Rev. B **57**, 1505 (1998).

[48] B. Meredig and C. Wolverton, Phys. Rev. B **80**, 245119 (2009).

[49] F. Zhou, T. Maxisch, and G. Ceder, Phys. Rev. Lett. **97**, 155704 (2006).

[50] C. B. Gopal and A. van de Walle, Phys. Rev. B **86**, 134117 (2012).

[51] S. Grieshammer, T. Zacherle, and M. Martin, Phys. Chem. Chem. Phys. **15**, 15935 (2013).

[52] S. S. Naghavi, A. A. Emery, H. A. Hansen, F. Zhou, V. Ozolins, and C. Wolverton, Nat. Commun. **8**, 285 (2017).

[53] M. Capdevila-Cortada and N. López, Nat. Mater. **16**, 328 (2017).

[54] A. Trovarelli, *Catalysis by Ceria and Related Materials* (Imperial College Press, London, 2002).

[55] M. Lumeij, J. Koettgen, M. Gilleßen, T. Itoh, and R. Dronskowski, Solid State Ionics **222–223**, 53 (2012).

[56] T. Zacherle, A. Schriever, R. A. De Souza, and M. Martin, Phys. Rev. B **87**, 134104 (2013).

[57] D. Frenkel and B. Smit, *Understanding Molecular Simulation. From Algorithms to applications* (Academic Press, San Diego, California, 2002), Vol. 1.

[58] E. A. Carter, G. Ciccotti, J. T. Hynes, and R. Kapral, Chem. Phys. Lett. **156**, 472 (1989).

[59] H. Eyring, J. Chem. Phys. **3**, 107 (1935).

[60] H. Eyring, S. H. Lin, and S. M. Lin, *Basic Chemical Kinetics* (Wiley, New York, 1980).

[61] M. Mantina, L. Q. Chen, and Z. K. Liu, Defect Diffus. Forum **294**, 1 (2009).

[62] G. Bussi, A. Laio, and M. Parrinello, Phys. Rev. Lett. **96**, 090601 (2006).

[63] S. Baroni, P. Giannozzi, and E. Isaev, Rev. Mineral. Geochem. **71**, 39 (2010).

[64] L. Gerward, J. Staun Olsen, L. Petit, G. Vaitheeswaran, V. Kanchana, and A. Svane, J. Alloys Compd. **400**, 56 (2005).

[65] M. Mogensen, T. Lindegaard, U. R. Hansen, and G. Mogensen, J. Electrochem. Soc. **141**, 2122 (1994).

[66] S. Rossignol, F. Gérard, D. Mesnard, C. Kappenstein, and D. Duprez, J. Mater. Chem. **13**, 3017 (2003).

[67] L. Gerward and J. S. Olsen, Powder Diffr. **8**, 127 (1993).

[68] H. Hayashi, M. Kanoh, C. J. Quan, H. Inaba, S. Wang, M. Dokiya, and H. Tagawa, Solid State Ionics **132**, 227 (2000).

[69] S. Grieshammer, M. Nakayama, and M. Martin, Phys. Chem. Chem. Phys. **18**, 3804 (2016).

[70] T. Zacherle, P. C. Schmidt, and M. Martin, Phys. Rev. B **87**, 235206 (2013).

[71] J. X. Zheng, G. Ceder, T. Maxisch, W. K. Chim, and W. K. Choi, Phys. Rev. B **73**, 104101 (2006).

[72] J. Wang, Y. Du, H. Xu, C. Jiang, Y. Kong, L. Sun, and Z.-K. Liu, Phys. Rev. B **84**, 024107 (2011).

[73] X. Li, M. W. Finnis, J. He, R. K. Behera, S. R. Phillpot, S. B. Sinnott, and E. C. Dickey, Acta Mater. **57**, 5882 (2009).

[74] J. P. Perdew, K. Burke, and M. Ernzerhof, Phys. Rev. Lett. **77**, 3865 (1996).

[75] P. E. Blöchl, Phys. Rev. B **50**, 17953 (1994).

[76] G. Kresse and J. Furthmüller, Phys. Rev. B **54**, 11169 (1996).

[77] G. Kresse and D. Joubert, Phys. Rev. B **59**, 1758 (1999).

[78] M. Nolan and J. E. W. G. W. Fearon, Solid State Ionics **177**, 3069 (2006).

[79] Z. Yang, G. Luo, Z. Lu, and K. Hermansson, J. Chem. Phys. **127**, 074704 (2007).

[80] Z. Yang, G. Luo, Z. Lu, T. K. Woo, and K. Hermansson, J. Phys.: Condens. Matter **20**, 035210 (2008).

[81] M. Nolan, V. S. Verdugo, and H. Metiu, Surf. Sci. **602**, 2734 (2008).

[82] J. Hooper, A. Ismail, J. B. Giorgi, and T. K. Woo, Phys. Rev. B **81**, 224104 (2010).

[83] G. Henkelman and H. Jónsson, J. Chem. Phys. **111**, 7010 (1999).

[84] A. Heyden, A. T. Bell, and F. J. Keil, J. Chem. Phys. **123**, 224101 (2005).

[85] E. Cockayne and B. P. Burton, Phys. Rev. B **62**, 3735 (2000).

[86] S. Fabris, G. Vicario, G. Balducci, S. de Gironcoli, and S. Baroni, J. Phys. Chem. B **109**, 22860 (2005).

[87] C. W. M. Castleton, J. Kullgren, and K. Hermansson, J. Chem. Phys. **127**, 244704 (2007).

[88] S. Nosé, J. Chem. Phys. **81**, 511 (1984).

[89] W. G. Hoover, Phys. Rev. A **31**, 1695 (1985).

[90] S. Fabris, S. de Gironcoli, S. Baroni, G. Vicario, and G. Balducci, Phys. Rev. B **71**, 041102 (2005).

[91] M. Nolan, S. Grigoleit, D. C. Sayle, S. C. Parker, and G. W. Watson, Surf. Sci. **576**, 217 (2005).

[92] J. L. F. Da Silva, M. V. Ganduglia-Pirovano, J. Sauer, V. Bayer, and G. Kresse, Phys. Rev. B **75**, 045121 (2007).

[93] M. Huang and S. Fabris, J. Phys. Chem. C **112**, 8643 (2008).

[94] D. Lu and P. Liu, J. Chem. Phys. **140**, 084101 (2014).

[95] M. Capdevila-Cortada, Z. Łodziana, and N. López, ACS Catal. **6**, 8370 (2016).

[96] D. E. Jiang and E. A. Carter, Phys. Rev. B **67**, 214103 (2003).

[97] Y.-S. Lee, Y. Kim, Y. W. Cho, D. Shapiro, C. Wolverton, and V. Ozoliņš, Phys. Rev. B **79**, 104107 (2009).

[98] See Supplemental Material at http://link.aps.org/supplemental/10.1103/PhysRevB.97.024305 for more information and complementary results.

[99] X. Li, Ph.D. thesis, The Pennsylvania State University, 2010.

[100] D. Y. Wang and A. S. Nowick, J. Solid State Chem. **35**, 325 (1980).

[101] Jülich Supercomputing Centre, J. Large-Scale Research Facilities **2**, A62 (2016).